

Magnetoexcitons in large area CVD-grown monolayer MoS₂ and MoSe₂ on sapphireA. A. Mitioglu,^{1,2} K. Galkowski,¹ A. Surrente,¹ L. Kłopotowski,³ D. Dumcenco,⁴ A. Kis,⁴ D. K. Maude,¹ and P. Plochocka^{1,*}¹Laboratoire National des Champs Magnétiques Intenses, CNRS-UGA-UPS-INSA, Grenoble and Toulouse, France²Institute of Applied Physics, Academiei Strasse 5, Chisinau, MD-2028, Republic of Moldova³Institute of Physics, Polish Academy of Sciences, al. Lotników 32/46, 02-668 Warsaw, Poland⁴Electrical Engineering Institute and Interdisciplinary Center for Electron Microscopy (CIME),

École Polytechnique Fédérale de Lausanne (EPFL), CH-1015 Lausanne, Switzerland

(Received 3 February 2016; revised manuscript received 24 March 2016; published 11 April 2016)

Magnetotransmission spectroscopy was employed to study the valley Zeeman effect in large area monolayer MoS₂ and MoSe₂. The extracted values of the valley g factors for both A and B excitons were found to be similar with $g_v \simeq -4.5$. The samples are expected to be strained due to the CVD growth on sapphire at high temperature (700 °C). However, the estimated strain, which is maximum at low temperature, is only $\simeq 0.2\%$. Theoretical considerations suggest that the strain is too small to significantly influence the electronic properties. This is confirmed by the measured value of the valley g factor, and the measured temperature dependence of the band gap, which are almost identical for CVD and mechanically exfoliated MoS₂.

DOI: [10.1103/PhysRevB.93.165412](https://doi.org/10.1103/PhysRevB.93.165412)**I. INTRODUCTION**

Monolayer transition metal dichalcogenides (TMDs) have recently emerged as an exciting material system in which coupled spin-valley physics can be explored [1–12]. Unlike their bulk form, monolayer TMDs exhibit a direct band gap in a visible spectral range located at two inequivalent $\pm K$ valleys [2,3]. The spin states are split by a strong spin-orbit interaction, and the order of the spin states is reversed in the $\pm K$ valleys as a result of time-reversal symmetry. Due to the large spin-orbit splitting, the interband optical absorption gives rise to well separated A- and B-exciton transitions. The selection rules for these transitions are governed by the orbital magnetic moment resulting from the Bloch part of the carrier wave function [13]. Since the crystal structure of a monolayer TMD lacks an inversion center, the out-of-plane element of the orbital magnetic moment is nonzero and its sign depends on the valley index. This results in optical transitions in σ^\pm polarizations, which involve carriers in the $\pm K$ valleys, providing an access to the valley index via optical spectroscopy [5–8]. Photoluminescence revealed a large degree of circular polarization [5–9], reaching 100% for a resonant excitation [6], which is extremely promising with a view to employing the valley pseudospin degree of freedom in novel applications in, e.g., quantum information processing [4–6,14]. In this respect, the development of large area monolayer TMDs suitable for large scale device applications is crucial.

The existence of a valley-contrasting magnetic moment opens a possibility of controlling the valley pseudospin with an external magnetic field [15–20]. The application of a magnetic field, perpendicular to the layer, lifts the valley degeneracy splitting the exciton transitions. In monolayer TMDs the magnetic moment of the carriers has three possible contributions, (i) intracellular $\mu_k = \pm 2\mu_B$ magnetic moment originating from the orbital contribution of the valence band d orbitals [21], (ii) the intercellular valley magnetic moment,

which is associated with the Berry curvature [4], and (iii) the spin Zeeman magnetic moment. As the optical transitions conserve spin, the spin magnetic moment does not contribute to the valley splitting. In a simple two-band model, the masses of the valence and the conduction band are identical so that the intercellular valley magnetic moment is the same for the valence and conduction bands. Thus, there is no intercellular contribution to the valley splitting which arises solely from the $\mu_k = \pm 2\mu_B$ angular momentum of the valence d orbitals giving a valley g factor $g_v = -4$, close to the reported values from photoluminescence (PL) studies in transition metal diselenides [20,22–26].

Surprisingly, a significant deviation from $g_v = -4$ was reported by Aivazian *et al.* [25]. A systematic study showed that the valley g factor can take values of either $\simeq -2.8$ or $\simeq -1.6$, depending on the sample. This was attributed to asymmetry between the conduction and valence bands, giving rise to different effective masses of electrons and holes, and thus different intercellular contributions to the valley moment. However, the origins of the asymmetry have not been identified. As the result was sample dependent, it was suggested that a natural candidate for influencing the band structure is strain or doping. However, the work by Li *et al.* [23] convincingly demonstrates that doping has no influence on the valley splitting. This leaves only strain as a possible candidate to influence the valley Zeeman splitting, in line with theoretical predictions showing that strain leads to asymmetry of the masses in the valence and the conduction band [27,28].

In this paper we present polarization resolved magneto-optical absorption measurements in the magnetic field up to 65 T on large area chemical vapor deposition (CVD) grown epitaxial monolayer molybdenum disulfide (MoS₂) and molybdenum diselenide (MoSe₂) samples. Using σ^\pm circularly polarized light we can individually address absorption to the $\pm K$ valleys. In contrast to photoluminescence measurements, which generally probe only the A exciton, absorption provides easy access to the higher energy B exciton which arises due to the large spin-orbit splitting of the valence band in TMDs. At low temperatures ($T \simeq 2$ K) and in a

*paulina.plochocka@lnm.cnrs.fr

magnetic field, both excitons exhibit a large splitting of the σ^\pm transitions with an effective valley g factor $g_v \simeq -4$ in agreement with previous magneto-optical investigations of the A exciton in exfoliated single layer TMDs [20,23,24,26]. The similar values for the valley g factor of the A and B excitons is in line with band structure calculations [11,29]. We find that for both excitons the value of the valley g factor is approximately independent of the temperature. In CVD grown samples, strain is naturally induced by the growth at high temperatures [30,31]. Our results demonstrate that the strain induced by the different coefficients of thermal expansion of the TMD and the sapphire substrate has a negligible influence on the electronic properties.

II. EXPERIMENTAL DETAILS

The large area monolayer molybdenum disulfide (MoS_2) and molybdenum diselenide (MoSe_2) samples have been obtained by the CVD method on highly polished sapphire substrates [30]. Prior to the growth, the substrates were cleaned by acetone/isopropanol/DI-water and further annealed at 1000°C in air for 1 h. The growth process is based on the gas-phase reaction between MoO_3 ($\geq 99.998\%$ purity, Alfa Aesar) and sulfur/selenium evaporated from solid phase ($\geq 99.99\%$ purity, Sigma Aldrich). A crucible, containing ~ 5 mg MoO_3 with the sapphire substrates placed facedown above it, was loaded into a 32 mm outer diameter quartz tube placed in a three-zone furnace. A second crucible located upstream from the growth substrates contained 350 mg of sulfur or 150 mg of selenium. Ultrahigh-purity argon (Ar) was used as the carrier gas, and CVD growth was performed at atmospheric pressure. The recipe for the MoS_2 growth is as follows; ramp the temperature to 300°C (200 sccm of Ar flow) and set 300°C for 10 min, ramp to 700°C with $50^\circ\text{C min}^{-1}$ rate (10 sccm of Ar) and set 700°C for 10 min, cool down to 570°C and open the furnace for rapid cooling (increase the Ar flow to 200 sccm). The initially triangular shaped monolayers of MoS_2 merge into a large area continuous film with typical dimensions of a few millimeters over $\simeq 1$ cm. For MoSe_2 , in addition to 10 sccm of Ar, 3 sccm of H_2 was introduced during 10 min growth at 700°C . More details concerning the growth can be found in the supplementary information section of Ref. [30].

Polarized-resolved magneto-optical measurements have been performed at different temperatures using 70 T long-duration pulsed magnet (~ 500 ms duration). A tungsten halogen lamp was used to provide a broad spectrum in the visible and near-infrared range. The absorption was measured in the Faraday configuration in which the light propagation vector k is parallel to the magnetic field B . Typical size of the spot was of the order of $200 \mu\text{m}$ which is much smaller compared to the dimensions of the monolayer TMD film. The circular polarization optics which allows us to selectively probe the transitions in one of the valleys was introduced *in situ*. To detect the opposite circular polarization, the magnetic field direction was reversed. In our work, the σ^\pm polarization was arbitrarily assigned to have a negative valley g factor in agreement with the literature. All spectra were normalized by the incident intensity to produce absolute transmission spectra.

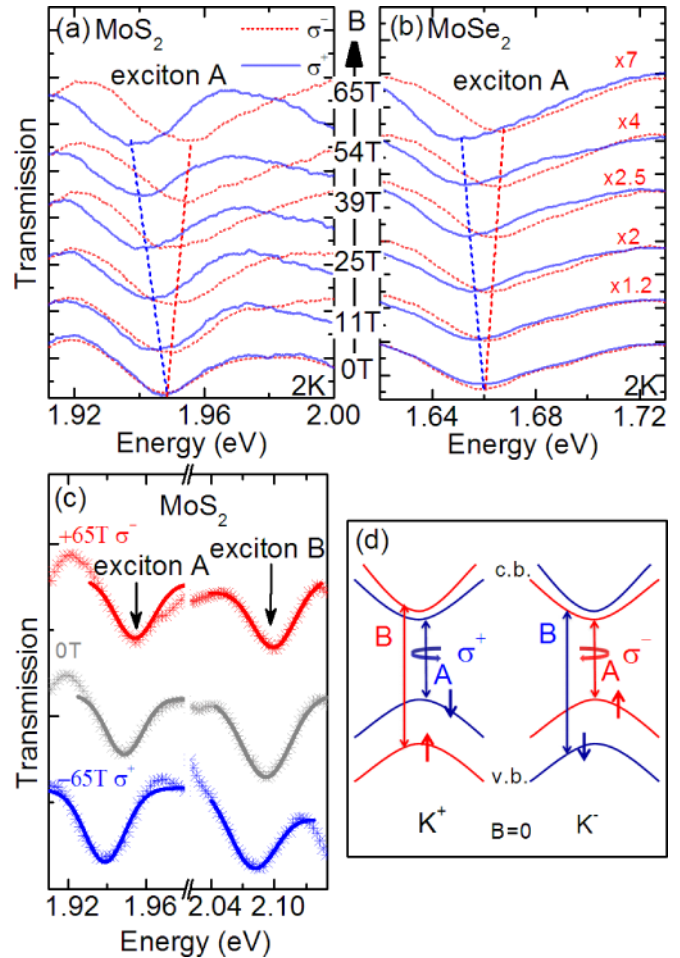


FIG. 1. (a) and (b) Typical low temperature transmission spectra for MoS_2 and MoSe_2 showing data obtained for σ^+ and σ^- polarization. (c) Example of the fitting Gaussian function to the spectra at $B = 0$ and ± 65 T. (d) Schematic showing the optical selection rules and the shift of the bands in the magnetic field.

III. MAGNETO-OPTICAL ABSORPTION SPECTROSCOPY

A. Valley g factors

Representative low temperature magnetotransmission spectra obtained for a single layer MoS_2 and MoSe_2 showing A-exciton absorption are presented in Figs. 1(a) and 1(b) for σ^+ and σ^- circular polarization. For MoSe_2 each σ^- spectra in the magnetic field has been multiplied by a suitable numerical factor to have a similar absorption intensity as the σ^+ spectra. The minima observed in all the spectra occurs at an energy corresponding to the expected A-exciton absorption in both materials [1].

A clear splitting of both exciton transitions is observed which increases linearly with increasing magnetic field and reaches about 18 meV at the maximum applied field (65 T). Such a splitting has been previously observed in PL measurements at lower magnetic field in exfoliated samples [1,20,22–25]. The valley splitting arises from the opposite sign of the valley magnetic moment in the valence band. The relative magnetic field induced energy shift of the valence and conduction band in each valley is schematically presented

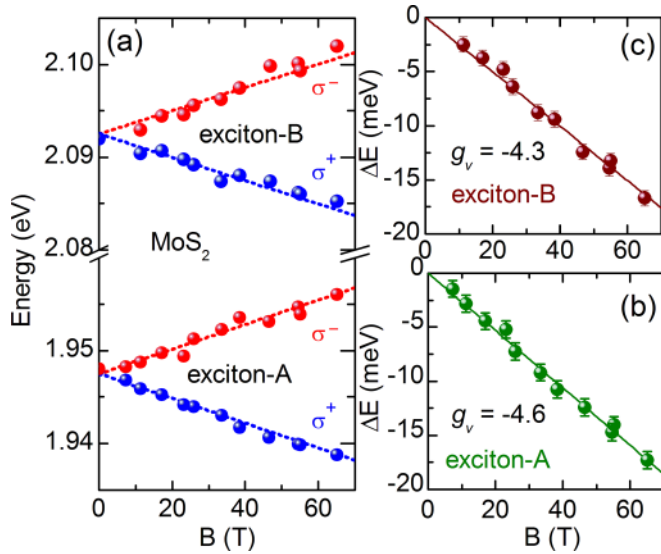


FIG. 2. (a) Transition energies for the A and B excitons in monolayer MoS₂ at $T = 2$ K. (b) and (c) The A and B exciton valley splitting at $T = 2$ K. The solid lines are linear fits used to extract the indicated valley g factors. The broken lines in (a) are the calculated evolution of the transition with magnetic field assuming a valley splitting of $\pm 0.5g_v\mu_B B$.

in Fig. 1(d). The dipole-allowed transitions for the A and B excitons are indicated by the vertical arrows. For both excitons σ^+ polarized light couples to the $+K$ valley while σ^- polarized light couples to the $-K$ valley. In the absence of a magnetic field, the $\pm K$ transitions have identical energies for both the A and B excitons. Applying a magnetic field breaks the time-reversal symmetry, lifting the valley degeneracy, which splits the $\pm K$ (σ^\pm) transitions. It is important to note that the schematic in the Fig. 1(d) is valid only for molybdenum dichalcogenides. For the tungsten dichalcogenides, the order of the spin up/down conduction bands is reversed [32].

To extract the exciton splitting energy at each magnetic field, the energy of the absorption line was determined by fitting a Gaussian function. Examples of the fitted spectra at $B = 0$ and 65 T for both circular polarizations are shown in Fig. 1(c). The spectra are shown for MoS₂ in the energy range covering both the A and B excitons. The energy of the A- and B-excitonic transitions as a function of magnetic field in monolayer MoS₂ is plotted in Fig. 2(a) for σ^\pm polarizations. For both excitons, the energy of the transitions evolve linearly with magnetic field.

The difference between the transition energy with σ^+ and σ^- circular polarized light ($\Delta E = E_{\sigma^+} - E_{\sigma^-}$) in magnetic field for both excitons is presented in Figs. 2(b) and 2(c). The exciton valley splitting scales linearly with the magnetic field and is almost identical for both excitons. A linear fit to the data gives $g_v \simeq -4.6 \pm 0.1$ and $g_v \simeq -4.3 \pm 0.1$ for the A and B excitons, respectively. Similar values for exciton A were reported for exfoliated monolayer MoSe₂ samples using photoluminescence measurements in low magnetic fields [22,23]. The expected evolution of the transition energies in magnetic field, calculated using the valley Zeeman splitting $\pm 0.5g_v\mu_B B$ is indicated in Fig. 2(a) by the broken lines.

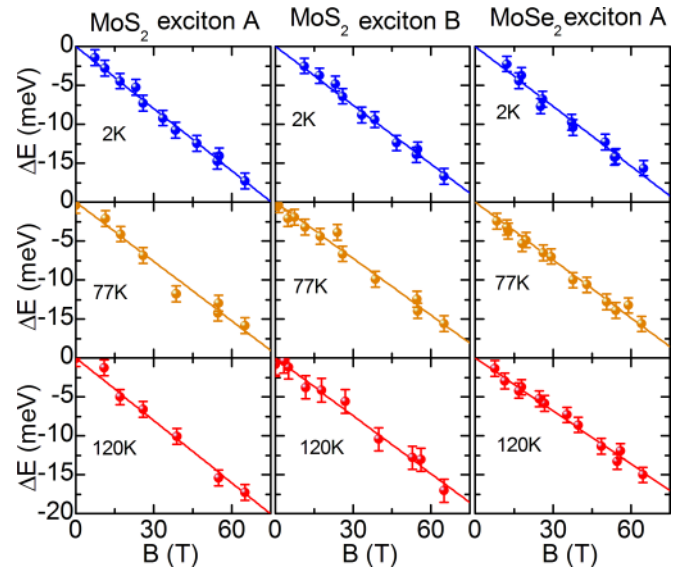


FIG. 3. The exciton valley splitting in monolayer MoS₂ and MoSe₂ for three different temperatures. The solid lines are linear fits to the data made to extract the valley g factors summarized in Table I.

The excellent agreement with the data confirms that within experimental error the splitting is symmetric with no evidence for a diamagnetic shift or cyclotronlike free carrier contribution to the magnetic field evolution of the transitions.

We have measured transmission spectra at $B = 0$ and $B = \pm 65$ T (σ^\pm) for three different temperatures for the A and B excitons in MoS₂ and A exciton in MoSe₂ (exciton B is not resolved in our CVD MoSe₂ samples). The precise position of the exciton transitions as a function of magnetic field was obtained by fitting Gaussian functions. The obtained splitting ΔE between the σ^+ and σ^- transitions is plotted in Fig. 3 versus the magnetic field at three different temperatures. The valley g factors were extracted by linear fits to the data (solid lines). The values of the temperature dependent valley g factor are summarized in Table I. In MoS₂, for both excitonic transitions, the valley g factor is independent of the temperature within experimental error. For MoSe₂, where only the exciton A is observed, the g factor is constant within experimental error for $T \leq 77$ K and decreases by around 10% at $T = 120$ K.

B. The influence of strain

Strain modifies the ratio of the effective masses in the valence and the conduction bands giving rise to an intercellular

TABLE I. Summary of the temperature dependence of the valley g factors for A and B excitons in MoS₂ and the A exciton in MoSe₂.

T (K)	MoS ₂ A	MoS ₂ B	MoSe ₂ A
2	-4.6 ± 0.1	-4.3 ± 0.1	-4.4 ± 0.1
77	-4.4 ± 0.1	-4.2 ± 0.1	-4.3 ± 0.1
120	-4.6 ± 0.1	-4.3 ± 0.1	-3.9 ± 0.1

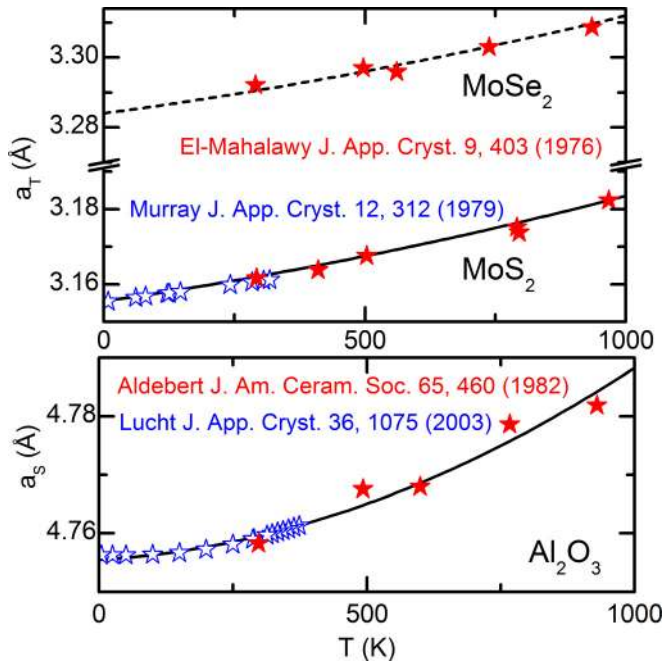


FIG. 4. Temperature dependence of the measured a lattice constant of bulk MoS₂, MoSe₂, and sapphire (Al₂O₃) taken from the literature [35–38]. Note that for the low temperature MoS₂ data, scatter was reduced by taking points corresponding to the linear fit to the data in Ref. [38]. The samples were grown at $T = 973$ K. The solid lines are fits to the data using second-order polynomials. The dashed line is the MoS₂ fit shifted vertically to coincide with the MoSe₂ high temperature data.

contribution to the valley splitting which then takes the form $\Delta E = 4\mu_B B - 2\Delta\alpha\mu_B B$, where $\Delta\alpha = (1/m_c - 1/m_v)$ and m_c, m_v are the effective masses in the conduction and valence band in the units of the free electron mass [21,25]. In principle $\Delta\alpha$ can be calculated taking into account higher order corrections to the tight-binding model. Estimations vary between 0.2 and 1.1 depending on if only nearest neighbor (NN) or next nearest neighbor (NNN) hopping parameters are taken into account in a three-band tight-binding model [21,25]. CVD grown samples are naturally strained [30,31], which results in the modification of the band structure, in particular the ratio of the effective masses in the valence and conduction bands [27,28,33,34].

To estimate the strain we need to know the temperature dependence of the lattice constant a of the bulk TMDs and sapphire from the lowest measurement temperature up to the growth temperature ($700^\circ\text{C} \equiv 973$ K) at which the TMD monolayer is assumed to be unstrained. In Fig. 4 we plot the a lattice constant assembling published data in the literature [35–38] in order to span the temperature range of interest for MoS₂, MoSe₂, and sapphire. The solid lines are second-order polynomial fits which we use to calculate the strain versus temperature. For MoSe₂ we were unable to find any published data below room temperature. Fortunately, the high temperature data suggests that the temperature dependence of MoS₂ and MoSe₂ are almost identical. We therefore use the fitted temperature dependence of MoS₂ which has been shifted vertically (broken line).

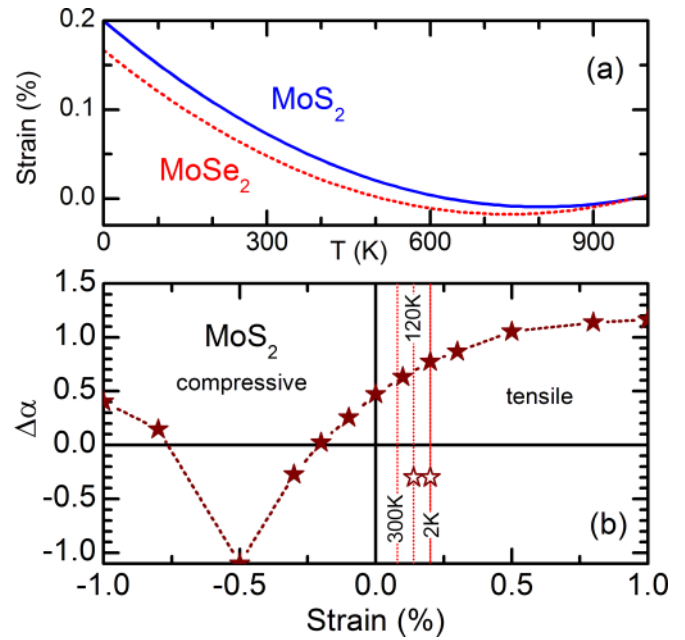


FIG. 5. (a) The calculated strain as a function of temperature due to the different thermal contraction of the TMD monolayer and the Al₂O₃ substrate. (b) Closed symbols show the calculated intercellular correction coefficient $\Delta\alpha$ for MoS₂ as a function of the strain. The open symbols show the required values of $\Delta\alpha$ to agree with the measured valley g factors.

The strain is by definition,

$$\varepsilon(T) = \frac{a'_T(T) - a_T(T)}{a_T(T)},$$

where $a'_T(T)$ is the lattice constant of the TMD grown on sapphire and $a_T(T)$ is the lattice constant of the unstrained bulk TMD. Assuming that the TMD monolayer is constrained to follow the thermal contraction of the sapphire substrate when the sample is cooled from the growth temperature, we can write

$$\frac{a'_T(T)}{a_T(973)} = \frac{a_S(T)}{a_S(973)},$$

where $a_S(T)$ is the lattice constant of the sapphire substrate. Thus, the strain is given by

$$\varepsilon(T) = \frac{a_S(T)a_T(973)}{a_S(973)a_T(T)} - 1,$$

which can be calculated using the polynomial approximations for the evolution of the lattice constants with temperature.

The calculated strain for MoS₂ and MoSe₂ is plotted in Fig. 5(a). For both TMDs the strain remains negligibly small as the sample is cooled from the growth temperature to 600 K. Below this temperature the tensile strain progressively increases reaching 0.2% in MoS₂ at low temperature. For MoSe₂ the strain is slightly smaller reaching a maximum value of $\simeq 0.17\%$ at $T = 0$ K.

In order to estimate the intercellular correction to the valley magnetic moment we have calculated $\Delta\alpha$ using the electron and hole effective masses at the K point in MoS₂, calculated as a function of strain, using density-functional

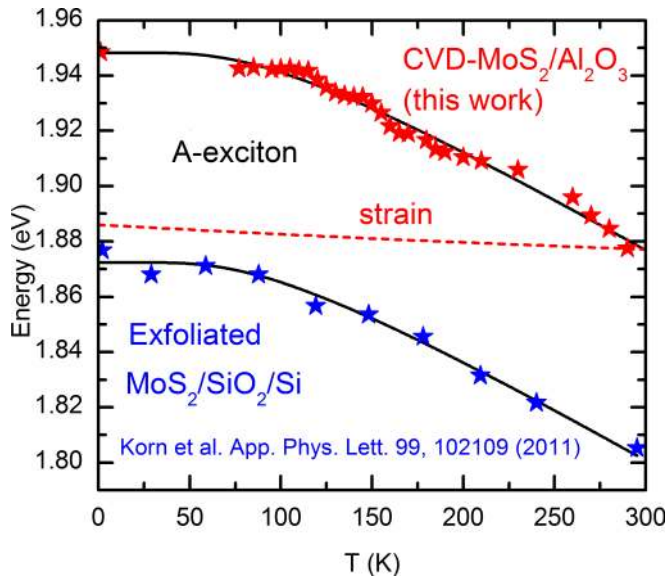


FIG. 6. The measured evolution of the A-exciton absorption in CVD MoS₂ on Al₂O₃. Data from the literature [41] for the A-exciton emission from exfoliated MoS₂ on SiO₂/Si substrate is shown for comparison. The solid lines are the fitted temperature dependence as described in the text. The broken line shows the calculated small contribution of the changing strain to the temperature dependence of CVD MoS₂ on Al₂O₃.

theory (DFT) [28]. The result is plotted as closed symbols in Fig. 5(b). The vertical broken lines indicate the expected strain in MoS₂ at 2 K, 120 K, and room temperature. While $\Delta\alpha$ varies little over the range of strain of interest, in line with the observation that the valley g factor remains almost unchanged with temperature, the value of $\Delta\alpha$, notably its sign, is not in agreement with the measured g factors with $g_v < -4$ which implies that $\Delta\alpha$ should be negative. The open symbols indicated the required values of $\Delta\alpha$ to have agreement with the experimental valley g factors. The failure of the DFT calculations to correctly predict the intercellular correction is not unexpected as excitons in TMDs are highly localized in real space, and thus delocalized in k space. This can in principle be taken into account by averaging the electron and hole effective masses over momentum space in the vicinity of the K points, which leads to a negative value of $\Delta\alpha$ in agreement with experiment [24]. However, such calculations are beyond the scope of this work.

Finally, the negligible influence of strain in CVD grown TMDs is confirmed by the temperature dependence of the A-exciton absorption in MoS₂ plotted in Fig. 6. We use the single oscillator model of O'Donnell and Chen to model the temperature dependence of the band gap [39]. The solid line is a fit to the data using

$$E(T) = E(0) - S \langle \hbar\omega \rangle \left[\coth \left(\frac{\langle \hbar\omega \rangle}{2KT} \right) - 1 \right],$$

where $\langle \hbar\omega \rangle = 24.25$ meV is the average phonon energy, $S = 2.29$ is a dimensional coupling constant, and $E(0) = 1.948$ eV is the low temperature band gap minus the exciton binding energy. The fit is excellent suggesting that strain plays little role in the observed temperature dependence. The expected variation of the band gap due to the change in strain with temperature, calculated from the measured $\simeq 70$ meV/% strain red shift in monolayer MoS₂ [40], is shown by the dashed line in Fig. 6. Clearly the expected strain-induced $\simeq 8$ meV change in the band gap is small compared to the observed $\simeq 70$ meV change with temperature.

For comparison, we plot the energy of the A-exciton emission in exfoliated MoS₂ on a SiO₂/Si substrate taken from the literature [41]. The energy of the emission is systematically shifted by $\simeq 72$ meV due to the different dielectric environment (exciton binding energy). The solid line through the data is calculated using the same parameters as for the CVD MoS₂ except for $E_0 = 1.872$ eV, which is shifted due to the increased exciton binding energy. The excellent agreement with experiment demonstrates that exfoliated and CVD MoS₂ have the same temperature dependence of the band gap, further confirming the negligible role played by strain in the latter.

IV. CONCLUSION

We have investigated large area monolayer MoS₂ and MoSe₂ samples, grown by CVD on sapphire, in high magnetic fields using optical absorption spectroscopy. The exciton valley splitting scales linearly with the magnetic field. In MoS₂ the extracted low temperature (2 K) valley g factors are $g_v \simeq -4.5 \pm 0.1$ for the A exciton and $g_v \simeq -4.3 \pm 0.1$ for the B exciton. In MoSe₂ for which only the A exciton was observed we find $g_v = -4.4 \pm 0.1$ at low temperatures. In both TMDs the g factor is almost independent of temperature over the available measurement range (2–120 K). The strain present at low temperature $\simeq 0.2\%$ in our CVD grown TMDs has little effect on the electronic properties. The low temperature valley g factors and the temperature dependence of the gap are identical to unstrained exfoliated MoS₂ on SiO₂/Si substrates. This suggests that the $\simeq 0.2\%$ tensile strain, which is naturally present in large area CVD grown Mo based TMDs on sapphire, does not represent any serious impediment for device applications.

During preparation of the manuscript we became aware of similar work on CVD grown WS₂ and MoS₂ monolayers by the NHMFL-Los Alamos group [42].

ACKNOWLEDGMENTS

This work was partially supported by ANR JCJC project milliPICS, the Region Midi-Pyrénées under Contract MESR13053031, STCU Project 5809, and the Swiss SNF Sinergia Grant No. 147607.

[1] Q. H. Wang, K. Kalantar-Zadeh, A. Kis, J. N. Coleman, and M. S. Strano, *Nat. Nanotechnol.* **7**, 699 (2012).

[2] K. F. Mak, C. Lee, J. Hone, J. Shan, and T. F. Heinz, *Phys. Rev. Lett.* **105**, 136805 (2010).

- [3] A. Splendiani, L. Sun, Y. Zhang, T. Li, J. Kim, C.-Y. Chim, G. Galli, and F. Wang, *Nano Lett.* **10**, 1271 (2010).
- [4] D. Xiao, G.-B. Liu, W. Feng, X. Xu, and W. Yao, *Phys. Rev. Lett.* **108**, 196802 (2012).
- [5] T. Cao, G. Wang, W. Han, H. Ye, C. Zhu, J. Shi, Q. Niu, P. Tan, E. W. B. Liu, and J. Feng, *Nat. Commun.* **3**, 887 (2012).
- [6] K. F. Mak, K. He, J. Shan, and T. F. Heinz, *Nat. Nanotechnol.* **7**, 494 (2012).
- [7] H. Zeng, J. Dai, W. Yao, D. Xiao, and X. Cui, *Nat. Nanotechnol.* **7**, 490 (2012).
- [8] G. Sallen, L. Bouet, X. Marie, G. Wang, C. R. Zhu, W. P. Han, Y. Lu, P. H. Tan, T. Amand, B. L. Liu, and B. Urbaszek, *Phys. Rev. B* **86**, 081301 (2012).
- [9] A. M. Jones, H. Yu, N. J. Ghimire, S. Wu, G. Aivazian, J. S. Ross, J. Yan, D. G. Mandrus, D. Xiao, W. Yao, and X. Xu, *Nat. Nanotechnol.* **8**, 634 (2013).
- [10] S. Wu, J. S. Ross, G.-B. Liu, G. Aivazian, A. Jones, Z. Fei, W. Zhu, D. Xiao, W. Yao, D. Cobden, and X. Xu, *Nat. Phys.* **9**, 149 (2013).
- [11] X. Xu, W. Yao, D. Xiao, and T. F. Heinz, *Nat. Phys.* **10**, 343 (2014).
- [12] K. F. Mak, K. L. McGill, J. Park, and P. L. McEuen, *Science* **344**, 1489 (2014).
- [13] W. Yao, D. Xiao, and Q. Niu, *Phys. Rev. B* **77**, 235406 (2008).
- [14] Z. Y. Zhu, Y. C. Cheng, and U. Schwingenschlögl, *Phys. Rev. B* **84**, 153402 (2011).
- [15] F. Rose, M. O. Goerbig, and F. Piéchon, *Phys. Rev. B* **88**, 125438 (2013).
- [16] T. Cai, S. A. Yang, X. Li, F. Zhang, J. Shi, W. Yao, and Q. Niu, *Phys. Rev. B* **88**, 115140 (2013).
- [17] A. Kormányos, V. Zólyomi, N. D. Drummond, and G. Burkard, *Phys. Rev. X* **4**, 011034 (2014).
- [18] Y.-H. Ho, Y.-H. Wang, and H.-Y. Chen, *Phys. Rev. B* **89**, 155316 (2014).
- [19] R.-L. Chu, X. Li, S. Wu, Q. Niu, W. Yao, X. Xu, and C. Zhang, *Phys. Rev. B* **90**, 045427 (2014).
- [20] A. A. Mitioglu, P. Plochocka, A. G. del Aguila, P. C. M. Christianen, G. Deligeorgis, S. Anghel, L. Kulyuk, and D. K. Maude, *Nano Lett.* **15**, 4387 (2015).
- [21] G.-B. Liu, W.-Y. Shan, Y. Yao, W. Yao, and D. Xiao, *Phys. Rev. B* **88**, 085433 (2013).
- [22] D. MacNeill, C. Heikes, K. F. Mak, Z. Anderson, A. Kormányos, V. Zólyomi, J. Park, and D. C. Ralph, *Phys. Rev. Lett.* **114**, 037401 (2015).
- [23] Y. Li, J. Ludwig, T. Low, A. Chernikov, X. Cui, G. Arefe, Y. D. Kim, A. M. van der Zande, A. Rigosi, H. M. Hill, S. H. Kim, J. Hone, Z. Li, D. Smirnov, and T. F. Heinz, *Phys. Rev. Lett.* **113**, 266804 (2014).
- [24] A. Srivastava, M. Sidler, A. V. Allain, D. S. Lembke, A. Kis, and A. Imamoglu, *Nat. Phys.* **11**, 141 (2015).
- [25] G. Aivazian, Z. Gong, A. M. Jones, R.-L. Chu, J. Yan, D. G. Mandrus, C. Zhang, D. Cobden, W. Yao, and X. Xu, *Nat. Phys.* **11**, 148 (2015).
- [26] G. Wang, L. Bouet, M. M. Glazov, T. Amand, E. L. Ivchenko, E. Palleau, X. Marie, and B. Urbaszek, *2D Mater.* **2**, 034002 (2015).
- [27] H. Rostami, R. Roldán, E. Cappelluti, R. Asgari, and F. Guinea, *Phys. Rev. B* **92**, 195402 (2015).
- [28] E. Scalise, M. Houssa, G. Pourtois, V. Afanasev, and A. Stesmans, *Physica E* **56**, 416 (2014).
- [29] A. Ramasubramaniam, *Phys. Rev. B* **86**, 115409 (2012).
- [30] D. Dumcenco, D. Ovchinnikov, K. Marinov, P. Lazic, M. Gibertini, N. Marzari, O. L. Sanchez, Y.-C. Kung, D. Krasnozhan, M.-W. Chen, S. Bertolazzi, P. Gillet, A. F. i Morral, A. Radenovic, and A. Kis, *ACS Nano* **9**, 4611 (2015).
- [31] Z. Liu, M. Amani, S. Najmaei, Q. Xu, X. Zou, W. Zhou, T. Yu, C. Qiu, A. G. Birdwell, F. J. Crowne, R. Vajtai, B. I. Yakobson, Z. Xia, M. Dubey, P. M. Ajayan, and J. Lou, *Nat. Commun.* **5**, 5246 (2014).
- [32] A. Kormányos, G. Burkard, M. Gmitra, J. Fabian, V. Zólyomi, N. D. Drummond, and V. Falko, *2D Mater.* **2**, 022001 (2015).
- [33] H. J. Conley, B. Wang, J. I. Ziegler, R. F. Haglund, S. T. Pantelides, and K. I. Bolotin, *Nano Lett.* **13**, 3626 (2013).
- [34] Q. Yue, J. Kang, Z. Shao, X. Zhang, S. Chang, G. Wang, S. Qin, and J. Li, *Phys. Lett. A* **376**, 1166 (2012).
- [35] P. Alderbert and J. P. Traverse, *J. Am. Ceram. Soc.* **65**, 460 (1982).
- [36] S. H. El-Mahalawy and B. L. Evans, *J. Appl. Crystallogr.* **9**, 403 (1976).
- [37] M. Lucht, M. Lerche, H.-C. Wille, Y. V. Shvyd'ko, H. D. Rüter, E. Gerda, and P. Becker, *J. Appl. Crystallogr.* **36**, 1075 (2003).
- [38] R. Murray and B. Evans, *J. Appl. Crystallogr.* **12**, 312 (1979).
- [39] K. P. O'Donnell and X. Chen, *Appl. Phys. Lett.* **58**, 2924 (1991).
- [40] K. He, C. Poole, K. F. Mak, and J. Shan, *Nano Lett.* **13**, 2931 (2013).
- [41] T. Korn, S. Heydrich, M. Hirmer, J. Schmutzler, and C. Schüller, *Appl. Phys. Lett.* **99**, 102109 (2011).
- [42] A. V. Stier, K. M. McCreary, B. T. Jonker, J. Kono, and S. A. Crocker, *Nat. Commun.* **7**, 10643 (2016).